DOI: 10.15587/978-617-8360-19-1.CH3

Vitalii Budashko, Oksana Glazeva, Albert Sandler,
Sergii Khniunin, Valentyn Bogach, Yurii Zhuravlov

CHAPTER 3

IMPROVEMENT OF THE METHOD OF LINEAR-QUADRATIC CONTROL OF AZIMUTHAL DRIVERS OF THE COMBINED PROPULSION COMPLEX

ABSTRACT

The development of the coastal shelf (mining of natural resources, construction of wind and tidal power plants, pelagic fishing, etc.) involves the development of high-tech, science-intensive branches of the marine industry, which involve the construction and operation of ships designed for exploration and drilling, lifting and transport and loading and unloading operations in various operating conditions (the so-called offshore fleet) [1, 2].

Comprehensive monitoring of degradation effects on the lines of propulsion flow has been carried out with the identification of corresponding markers at the intersections of energy flows.

Strategies for all-mode control of power, torque and speed of electric motors of azimuth thrusters (ATS) located in the stern of the combined propulsion complex (CPC) have been developed. Methods for constructing multi-criteria three-level power distribution control strategies in PPC ship power plants (SPP) are proposed [3, 4]. Taking this into account, the following objectives were solved within the framework of the study:

– based on the analysis of the CPC behavior and the ATS efforts in combination with studies of the design features of ships of a similar class, a mathematical model was determined that describes the behavior of the CPC with the ATS in the stern;

– based on the analysis of the principles of modeling and linearization of the ATS control systems and existing methods, the shapes of the state space were determined and the influence of disturbing forces on the characteristics of the controller was tracked;

– physical modeling of the multifunctional CPC with the ATS in the stern was carried out;

– the mathematical model was adapted to the algorithm of the controller and the control system with the corresponding testing of the controller using simulation modeling.

The parametric optimization of the linear-quadratic control of the CPC ATS allowed to increase the efficiency of the CPC SPP operation.

KEYWORDS

Combined propulsion complex, thruster, linear-quadratic control, modeling.

Azimuth thrusters (ATs) are a growing trend in the modern market of sea-based vehicles (SBVs). The AT is a propeller mounted in a nacelle under the SBV hull [5]. This nacelle is capable of rotating around its axis, which allows changing the direction of the force acting on the SBV. This chapter explores the possibilities of improving the control algorithms of large-scale SBV models using the linear-quadratic control principle and linearized hydrodynamics using the example of a model of a multifunctional propulsion complex [6, 7—9] with two ATs in the stern. The controller uses estimates of linear speeds and angular speeds obtained using the Global Positioning System (GPS) and Inertial Measurement Units (IMU) to control the SUV. The input signals are the azimuthal propeller speeds and the angles of the AT stops relative to the SBV diametrical plane. The SBV model is nonlinear in three main parameters: centripetal and Coriolis forces, hydrodynamic damping, and AT input parameters. All these effects are assumed to be approximately linear around the operating points of the controllers [10, 11]. The models are designed to integrate with two different controllers, one of which controls both ATs simultaneously, and the other with differential control. To verify the proposed controllers, simulations are performed where the step responses of the closed-loop system to overload and rotation speed are compared. The first is to verify the model, and the second is to observe how adequately the model and controllers work together [12, 13]. Simulations of speed jumps showed a fairly good response, but the propeller speed showed a more significant effect on the system than the orientation of the motors. When simulating the yaw speed, the behavior of the azimuth angle did not comply with the circular constraints inherent in a device rotating at the appropriate frequency. The calculated angles reached values greater than 2π, which, according to the trigonometric function, gives the same result as the zero angle. In other words, the forces will depend linearly on the azimuth angle. It is concluded that this is a result of the linearization of the actuators, and the proposed solution is to implement a setting reinforcement to better adapt to the AT rotational behavior [14, 15—17]. Another circumstance that contributes to this result is the decoupling between the speed throws, the swing speed and the yaw speed predicted by the linear controller. This is a problem, since in reality they will have some influence on each other. It is concluded that this is the result of using an overly simplified model or an unsuccessfully chosen operating point of the centripetal and Coriolis linearization. Despite these problems, the simulations showed the potential of the model and controller for use in similar situations [18, 19]. Several modifications are also proposed to significantly improve the model and simulations. One of the main changes that could be made is the implementation of predictive control during the linearization of the azimuth motor. This will lead to the fact that the propeller speed will have a greater impact on the directional forces, and the SBV behavior will be more predictable [20, 21].

Unlike the SBV with the AT, most modern ships are propelled by a mechanical system with an internal combustion motor (ICE) or a propeller electric motor (PEM), which drives an underwater propeller (**Fig. 3.1**). The direction of rotation of the propeller is usually fixed relative to the hull of the ship, and control is carried out mainly by a rudder in the stern. Some ships also have a tunnel thruster (TT), installed in the bow or stern and directed sideways to improve maneuverability, for example, when mooring. Another method of movement and maneuvering currently used is the AT. In this system, the propeller is mounted in a nacelle, which is itself mounted under the hull in such a way that it can rotate around a vertical axis. The propeller is driven by a mechanical transmission that connects it to an motor inside the ship or to a PEM installed inside the nacelle itself. This method of motion eliminates the need for a rudder and provides better maneuverability

of the ship in tight sailing conditions [22, 23]. With greater maneuverability, more scenarios for controlling the AT located in the stern appear, which require a more skilled operator or a more complex control system. This chapter describes the study of how adequately a smaller ship with an AT can be controlled using a linear quadratic regulator (LQR). This will require mathematical modeling of both the AT behavior and the behavior of the propeller thrust. Since LQR requires linear models for design, some simplifications and linearizations will be required. Thus, a linearized model will also be implemented to describe the motion of this AT type. The procedure for finding the optimal LQR that can control SBV with the AT in the stern is reduced to comparing its performance with real conditions based on the simulation results. To achieve the result, it is necessary to perform the following objectives in order to get a more complete understanding of the problem:

– determine a mathematical model that describes the behavior of the SBV with the AT in the stern under conditions of incomplete information;

– adapt the obtained mathematical model to work with the LCR in accordance with the algorithmization of the motion controller functioning;

– conduct physical modeling of the SBV with the AT the stern;

– conduct simulation studies that verify the capabilities of the proposed method.

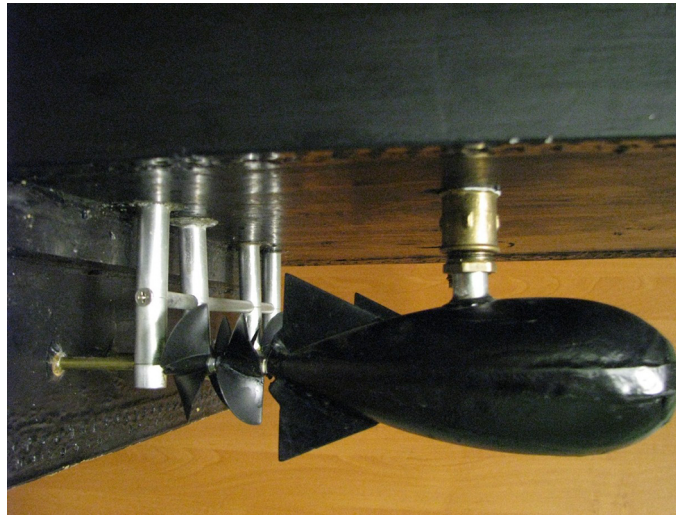

Fig. 3.1 Appearance of the AT physical model located in the stern of the physical model of the multifunctional propulsion complex with a variable structure

To solve the main problem, the main method was divided into five stages:

– analysis of the behavior of seagoing ships and AT efforts in combination with studies of the design features of modern ships of a similar class;

– analysis of the principles of modeling and linearization of AT control systems based on a review of existing methods;

– determination of the shape of the state space and tracking the influence of disturbing forces on the characteristics of the controller;

– testing the controller using simulation;

– analysis of the simulation results and possible changes in the controller settings.

To take into account the existing limitations, it was necessary to make a number of simplifications. Some degrees of freedom (DOF) were excluded, since they were determined to have little effect on the system. Thus, only 3 of the 6 degrees of freedom (DOF) were used in the simulation (sway, pitch, and yaw). Some parts of the resulting mathematical model will be nonlinear, so some linearization is required to make the model work with LQR. In the event that data from a real ship cannot be obtained, the simulation and development of the controller are performed using only nominal values.

The physical simulation begins with defining the coordinate system of the SBV and how certain forces act on the SBV in the aquatic environment. This is followed by an explanation of how the thrust and torque of the AT affect the SBV depending on the angle and speed of rotation. These mathematical models are then combined to form a spatial state vector in which the controller will be applied. This is followed by a description of how LQR works and how to find the optimal controller using the model and the Riccati equations. It is also explained how the subsequent actions of the controller are triggered depending on possible changes in operating conditions. The results of the simulation study with the regulator and controller settings of the reference input signals are analyzed in accordance with the achievement of the desired results. Also, during the simulation, the advantages of choosing different operating points for linearizing the model for different regulator settings are investigated.

3.1 DETERMINATION OF THE MOTION MODEL OF A MARINE VEHICLE UNDER CONDITIONS OF INCOMPLETE INFORMATION

To determine the position, orientation and speed of a marine vehicle, appropriate coordinate systems are required. These are the moving and stationary coordinate systems, which are defined in equations (3.1) and (3.2). The most common representation for the stationary coordinate system is based on the hull symmetry around the X_bZ_b-plane, the approximate symmetry around the Y_bZ_b-plane and the projection onto the Z_b-axis relative to the water surface, as shown in **Fig. 3.2**. The inertial (stationary) coordinate system is used to describe the position and orientation of the ship in global coordinates and Euler angles, as $[x\ y\ z]^T$ and $[\phi\ \theta\ \psi]^T$, respectively. The moving coordinate system describes the forces, torques, linear speeds and angular speeds $[X\ Y\ Z]^T$, $[K\ M\ N]^T$, $[u\ v\ w]^T$, $[x\ y\ z]^T$, and also $[p\ q\ r]^T$, respectively. The motion of a ship can be described by six degrees of freedom, which are divided into two categories: translational motion in three directions: longitudinal displacement (splash), transverse displacement (drift) and vertical displacement (lift), and rotational motion about three axes: roll, pitch and yaw. These are standard notations used in the modeling of marine ships [24].

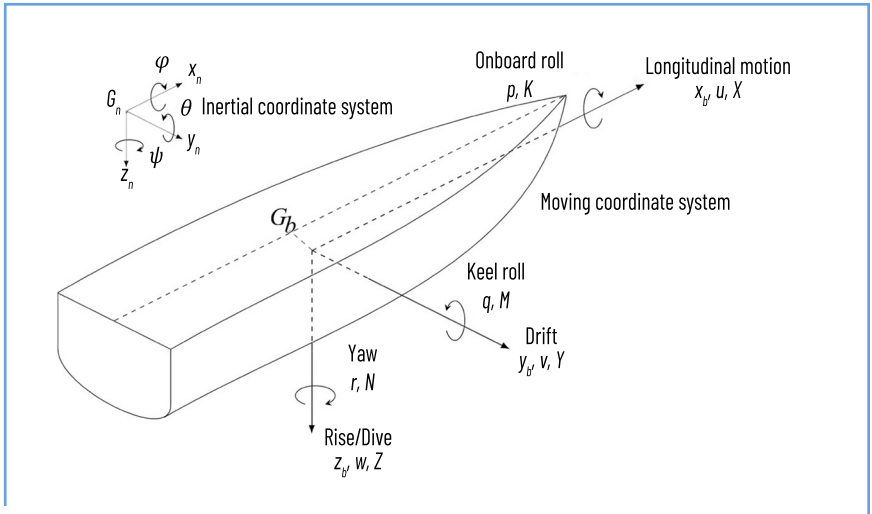

Fig. 3.2 Standard notation for describing the ship's motion according to (3.1) and (3.2)

LINEARIZATION OF THE SHIP'S MANEUVERING MODEL

A common simplification of the model is to neglect vertical motions and longitudinal roll. To obtain a simple model, the roll angle is also assumed to be small. With this in mind, the position orientation vector and the linear-angular speed vector can be defined as:

$$\eta \triangleq \left[x\ y\ \varphi\right]^T, \tag{3.1}$$

$$\nu \triangleq \left[u\ v\ r\right]^T. \tag{3.2}$$

These generalized positions and speeds have a geometric relationship that can be described as

$$\eta = J\left(\eta\right)\nu, \tag{3.3}$$

and the equations of motion of the ship in a fixed coordinate system are as follows

$$M_{RB}\nu = C_{RB}\left(\nu\right)\nu + D\left(\nu\right)\nu = \tau_{act}, \tag{3.4}$$

where M_{RB} – the inertia matrix of the rigid body; $C_{RB}(\nu)\nu$ – the centripetal and Coriolis terms; $D(\nu)$ – the damping matrix; τ_{act} – the vector with generalized external forces.

Initially, for this simple model, the Coriolis terms and the damping matrix will be approximated by a linear function. This system of equations of motion is based on, and the various descriptions of forces are based on [*n*], where models with four degrees of freedom (where roll is an additional degree of freedom) are studied, and not with three, as in our case. For three degrees of freedom, the equations are presented in the following form [25]:

$$J(\eta)=\begin{bmatrix}\cos\varphi & -\sin\varphi & 0\\ \sin\varphi & \cos\varphi & 0\\ 0 & 0 & 1\end{bmatrix}, \tag{3.5}$$

$$M_{RB}=\begin{bmatrix}m & 0 & -y_G\\ 0 & m & mx_G\\ -mx_G & mx_G & I_Z\end{bmatrix}, \tag{3.6}$$

$$C_{RB}(\nu)=\begin{bmatrix}0 & -mr & -mx_Gr\\ mr & 0 & -my_Gr\\ mx_Gr & my_Gr & I_0\end{bmatrix}, \tag{3.7}$$

$$D(\nu)=\begin{bmatrix}X_u & 0 & 0\\ 0 & Y_v & 0\\ 0 & 0 & N_r\end{bmatrix}, \tag{3.8}$$

where the total mass of the ship is taken as m, $r_g = r_G = [x_G, y_G]$; I_z is the moment of inertia about the z-axis, expressed in the b-system; X_u, Y_v and N_r – the scaling damping factors.

LINEARIZATION OF THE FORCE AND MOMENT MODELS OF THE AZIMUTH THRUSTER

On a classic seagoing ship, the driving forces come from the rudder, fixed propellers and thrusters. However, since the type of ship under consideration is driven by AT, the response to the application of forces will be different. The AT is a motor that can rotate 360 degrees around its vertical axis. This allows forces to be applied in the x- and y-directions depending on the AT position and the torque applied to the ship. The following model calculations, which use the input data of the rotation speed and the azimuth angle, are mainly derived from the model calculations used by Ljungberg. One, these approaches were improved by Liang and Andreas, who pay more attention to the azimuthal forces as input data, rather than the rotational speed [26, 27].

Let's suppose that the force N_a of the AT is applied to the ship hull. Let the thruster i be the AT rotating with the propeller speed n_i, and the angle of the applied resultant force α_i. Then the forces in the x_b-direction from the azimuthal motor i can be denoted as (**Fig. 3.3**)

$$F_{x,i} = g_x\left(n_i, \alpha_i, u_{a,i}\right), \tag{3.9}$$

where $u_{a,i}$ – the speed of water passing through the AT in the negative x_b direction. This is necessary because at higher speeds, and when $u_{a,i}$ and $n_i\ cos(\alpha_i)$ have the same sign, there will be efficiency losses. The assumption in the model is a linear relationship between g_x and n_i as

$$g_x\left(n_i, \alpha_i, u_{a,i}\right) = \mu_i n_i \cos\left(\alpha_i\right) - k_i' n_i u_{a,i} \cos\left(\alpha_i\right), \tag{3.10}$$

where μ_i and k_i – positive constants determined by field experiment, and $u_{a,i}$ can be described as

$$u_{a,i} = \left(1-\omega_i\right) u_r. \tag{3.11}$$

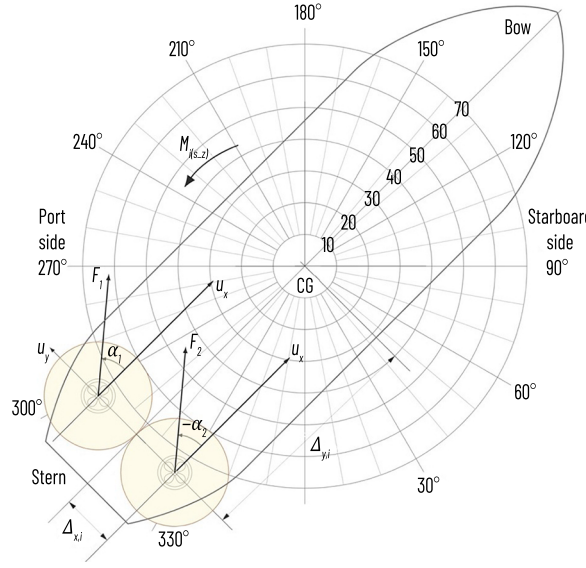

Fig. 3.3 Position and angle of rotation of motor *i*

Here, ω_i – the co-current coefficient, which defines the ratio of the speed of water flowing through the propeller to the speed of the ship u_r – the relative speed between the ship and the surrounding water. Combining the co-current coefficient, it is possible to simplify the second term of (3.10) using

$$k_i = \left(1-\omega_i\right) k_i', \tag{3.12}$$

and substituting this into (3.10)

$$g_x\left(n_i,\alpha_i,u_r\right)=\mu_i n_i\cos\left(\alpha_i\right)-k_i n_i u_r\cos\left(\alpha_i\right). \tag{3.13}$$

Thus, there is a generalized model of the forces from the AT. However, the true function $g_x(\bullet)$ is more complex due to water dynamics, but the approximate function will be adequate for the purposes of this study [28].

Similarly, the force in the Y_b-direction

$$F_{y,i}=g_y\left(n_i,\alpha_i,u_r\right)=\mu_i n_i\sin\left(\alpha_i\right)-k_i' n_i v_{a,i}\sin\left(\alpha_i\right)=\mu_i n_i\sin\left(\alpha_i\right)-k_i n_i u_r\sin\left(\alpha_i\right), \tag{3.14}$$

can be found under the same assumptions as for the *x*-direction. The azimuth motor *i* will also create a torque relative to the ship depending on where it is mounted relative to the ship's center of rotation. The torque can be described as

$$M_i=\Delta_{x,i}F_{y,i}-\Delta_{y,i}F_{x,i}. \tag{3.15}$$

The generalized torque vector is

$$\tau_{act}=\begin{bmatrix}\sum_{i=1}^{N_a}\mu_i n_i\cos\left(\alpha_i\right)-k_i n_i u_r\cos\left(\alpha_i\right)\\ \sum_{i=1}^{N_a}\mu_i n_i\sin\left(\alpha_i\right)-k_i n_i u_r\sin\left(\alpha_i\right)\\ \sum_{i=1}^{N_a}n_i\left[\mu_i\left(\Delta_{x,i}\sin\left(\alpha_i\right)-\Delta_{y,i}\cos\left(\alpha_i\right)\right)-k_i\left(\Delta_{x,i}v_r\sin\left(\alpha_i\right)-\Delta_{y,i}u_r\cos\left(\alpha_i\right)\right)\right]\end{bmatrix}, \tag{3.16}$$

contains the forces and moments from all the azimuthal motors added together. To make the model even simpler, it is possible to neglect the high-speed losses in the 4 direction, since the speeds in this direction are much lower than in the x_b direction.

Also, for simplicity, it is assumed that each motor is equally efficient, and therefore:

$$\mu_i=\mu_j\triangleq\mu\forall i,j=1,N_a, \tag{3.17}$$

$$k_i=k_j\triangleq k\forall i,j=1,N_a. \tag{3.18}$$

Which gives

$$\tau_{act} = \begin{bmatrix} \sum_{i=1}^{N_a} \mu n_i \cos(\alpha_i) - k n_i u_r \cos(\alpha_i) \\ \sum_{i=1}^{N_a} \mu n_i \sin(\alpha_i) \\ \sum_{i=1}^{N_a} \mu n_i \left[\Delta_{x,i} \sin(\alpha_i) - \Delta_{y,i} \cos(\alpha_i)(1 - k u_r) \right] \end{bmatrix}. \quad (3.19)$$

Since τ_{act} depends on u_r, which in turn depends on the rate of drag increase, the model becomes nonlinear. For simplicity, it is possible to neglect these terms and the notation of the generalized torque vector can be simplified to

$$\tau_{act} = \begin{bmatrix} \mu\tilde{\tau}_x \\ \mu\tilde{\tau}_y \\ \mu\tilde{\tau}_\varphi \end{bmatrix} = \begin{bmatrix} \mu \sum_{i=1}^{N_a} n_i \cos(\alpha_i) \\ \mu \sum_{i=1}^{N_a} n_i \sin(\alpha_i) \\ \mu \sum_{i=1}^{N_a} n_i \left[\Delta_{x,i} \sin(\alpha_i) - \Delta_{y,i} \cos(\alpha_i) \right] \end{bmatrix}. \quad (3.20)$$

3.2 ITERATIVE ADAPTATION OF SHIP MOTION MODELS IN ACCORDANCE WITH THE ALGORITHMIZATION OF THE MOTION CONTROLLER FUNCTIONING

LINEARIZATION OF CONTROLLER STATES

Since $C_{RB}(\nu)$ depends on ν, the $C_{RB}(\nu)\nu$ term becomes nonlinear. However, the use of LQR requires a linear model. Thus, linearization is needed to simplify the model further. The linearization is described by the function

$$L(x) = f(a) + f'(a)(x - a), \quad (3.21)$$

where $L(x)$ – the linearized function; $f(a)$ – the function to be linearized evaluated at a; $f'(a)$ – the derivative of $f(x)$ with respect to x evaluated at (a), in this case the Jacobian of the function $f(x)$. Finally, x – the linearization variable (in this case ν), a – the chosen operating point. In this case, the linearizing terms are:

$$f(\nu) = C_{rb}(\nu)\nu = \begin{bmatrix} 0 & -mr & -mx_G r \\ mr & 0 & -my_G r \\ mx_G r & my_G r & 0 \end{bmatrix} \begin{bmatrix} y \\ \nu \\ r \end{bmatrix}, \quad (3.22)$$

$$f(\nu)=\begin{bmatrix} -mr-mx_G r^2 \\ mr\nu-my_G r^2 \\ mx_G ru+my_G r\nu \end{bmatrix}, \tag{3.23}$$

which contain the Jacobian

$$J(\nu)=\begin{bmatrix} 0 & -mr & -mr-2mx_G r \\ mr & 0 & mu-2my_G r \\ mx_G r & my_G r & mx_G u=my_G \nu \end{bmatrix}. \tag{3.24}$$

The operating point depends on the state the system should be in. Since the system will operate at a constant forward speed and with small changes in the AT rotation speed, the corresponding operating point is defined as

$$a=\begin{bmatrix} u_0 \\ \nu_0 \\ r_0 \end{bmatrix}=\begin{bmatrix} 1 \\ 0 \\ 0 \end{bmatrix}. \tag{3.25}$$

Using this operating point and linearizing $C_{RB}(\nu)\nu$, let's find the following

$$L(\nu)=\begin{bmatrix} 0 & 0 & 0 \\ 0 & 0 & m \\ 0 & 0 & mx_G \end{bmatrix}=\begin{bmatrix} u \\ \nu \\ r \end{bmatrix}. \tag{3.26}$$

Then the state matrix (3.26) will replace $C_{RB}(\nu)\nu$ in the state space equation.

LINEARIZATION OF MOTION CONTROLLER INPUT SIGNALS

To control a ship using an AT, it is necessary to process the actuator signals as input signals, so the full equation (3.20) must be combined into a controller with a dependence on n and α. Due to the trigonometric functions cos and sin that are present in (3.21), linearization with the LQR framework is required to make it consistent.

The general case linearization is as follows. Since there are several operating points that can be selected in the simulation, a general case linearization is required. In addition, two different linearizations are required due to the two ways of controlling the ship. One with synchronous control, i.e. the same input signals for both AT, and one with differential (asynchronous) control, where the ATs are controlled independently. Starting with synchronous control, let's use the following variables

$$P_s = \begin{bmatrix} n_i \\ \alpha_i \end{bmatrix}. \tag{3.27}$$

Then (3.21) is integrated into (3.21) with the previously mentioned variable and the generalized operating point a_s:

$$f(p) = \tau(p) = \begin{bmatrix} \sum_{i=1}^{N_a} n_i \cos(\alpha_i) \\ \sum_{i=1}^{N_a} n_i \sin(\alpha_i) \\ \sum_{i=1}^{N_a} n_i \left(\Delta_{x,i} \sin(\alpha_i) - \Delta_{y,i} \cos(\alpha_i) \right) \end{bmatrix}, \tag{3.28}$$

$$J(p) = \sum_{i=1}^{N_a} \begin{bmatrix} \cos(\alpha_i) & -n_i \sin(\alpha_i) \\ \sin(\alpha_i) & n_i \cos(\alpha_i) \\ \Delta_{x,i} \sin(\alpha_i) - \Delta_{y,i} \cos(\alpha_i) & \Delta_{x,i} \sin(\alpha_i) + \Delta_{y,i} \cos(\alpha_i) \end{bmatrix}, \tag{3.29}$$

$$a_s = \begin{bmatrix} \bar{n} \\ \bar{\alpha} \end{bmatrix}. \tag{3.30}$$

which gives the following equation, which includes a constant term

$$L(p) = \sum_{i=1}^{N_a} \begin{bmatrix} \bar{n}\cos\bar{\alpha} \\ \bar{n}\sin\bar{\alpha} \\ \bar{n}\left(\Delta_{x,i} \sin\bar{\alpha} - \Delta_{y,i} \cos\bar{\alpha} \right) \end{bmatrix} + \sum_{i=1}^{N_a} \begin{bmatrix} \cos\bar{\alpha} & -\bar{n}\sin\bar{\alpha} \\ \sin\bar{\alpha} & \bar{n}\cos\bar{\alpha} \\ \left(\Delta_{x,i} \sin\bar{\alpha} - \Delta_{y,i} \cos\bar{\alpha} \right) & \left(\Delta_{x,i} \sin\bar{\alpha} + \Delta_{y,i} \cos\bar{\alpha} \right) \end{bmatrix} \begin{bmatrix} y'n \\ \bar{\alpha} \end{bmatrix}. \tag{3.31}$$

This means that the AT steady state must be at this operating point and the controller will control the deviation from this state. In other words, τ_{act} can be divided into two parts as follows

$$\tau_{act} = \bar{\tau}_{act} + \tilde{\tau}_{act}, \tag{3.32}$$

where $\bar{\tau}_{act}$ – a constant, and

$$\tilde{\tau}_{act} = \sum_{i=1}^{N_a} \begin{bmatrix} \cos\bar{\alpha} & -\bar{n}\sin\bar{\alpha} \\ \sin\bar{\alpha} & \bar{n}\cos\bar{\alpha} \\ \left(\Delta_{x,i}\sin\bar{\alpha} - \Delta_{y,i}\cos\bar{\alpha}\right) & \left(\Delta_{x,i}\sin\bar{\alpha} + \Delta_{y,i}\cos\bar{\alpha}\right) \end{bmatrix} \begin{bmatrix} n \\ \alpha \end{bmatrix}, \tag{3.33}$$

depends on time, which will be determined by the LQ controller. This linearization will force the AT to use the same rotation speed and propeller flow direction angle for both ATs.

For differential (asynchronous) control, the control variable will contain a separate definition of the control signal

$$P_d = \left[n_1\, n_2\, \alpha_1\, \alpha_2\right]^T. \tag{3.34}$$

As before, equation (3.21) is applied and a new Jacobi matrix is derived and the operating point is used. However, for *f(p)* (3.28) is still chosen, since these equations must also undergo the linearization procedure. The revised equations have the form:

$$J(p_d) = \begin{bmatrix} \cos\alpha_1 & \sin\alpha_1 & \Delta_{x,1}\sin\alpha_1 - \Delta_{y,1}\cos\alpha_1 \\ \cos\alpha_2 & \sin\alpha_2 & \Delta_{x,2}\sin\alpha_2 - \Delta_{y,2}\cos\alpha_2 \\ -n_1\sin\alpha_1 & n_1\cos\alpha_1 & n_1\left(\Delta_{x,1}\cos\alpha_1 - \Delta_{y,1}\sin\alpha_1\right) \\ n_2\sin\alpha_2 & n_2\cos\alpha_2 & n_2\left(\Delta_{x,2}\cos\alpha_2 - \Delta_{y,2}\sin\alpha_2\right) \end{bmatrix}, \tag{3.35}$$

$$a_d = \left[\bar{n}_1\, \bar{n}_2\, \bar{\alpha}_1\, \bar{\alpha}_2\right]^T. \tag{3.36}$$

These transformations give a complete linearization

$$L(p_d) = \begin{bmatrix} \bar{n}_1\cos\bar{\alpha}_1 + \bar{n}_2\cos\bar{\alpha}_2 \\ \bar{n}_1\sin\bar{\alpha}_1 + \bar{n}_2\sin\bar{\alpha}_2 \\ \bar{n}_1\left(\Delta_{x,1}\sin\bar{\alpha}_1 - \Delta_{y,1}\cos\bar{\alpha}_1\right) + \bar{n}_2\left(\Delta_{x,2}\sin\bar{\alpha}_2 - \Delta_{y,2}\cosn\bar{\alpha}_2\right) \end{bmatrix} +$$

$$+ \begin{bmatrix} \cos\bar{\alpha}_1 & \sin\bar{\alpha}_1 & \Delta_{x,1}\sin\bar{\alpha}_1 - \Delta_{y,1}\cos\bar{\alpha}_1 \\ \cos\bar{\alpha}_2 & \sin\bar{\alpha}_2 & \Delta_{x,2}\sin\bar{\alpha}_2 - \Delta_{y,2}\cos\bar{\alpha}_2 \\ -\bar{n}_1\sin\bar{\alpha}_1 & \bar{n}_1\cos\bar{\alpha}_1 & \bar{n}_1\left(\Delta_{x,1}\cos\bar{\alpha}_1 + \Delta_{y,1}\sin\bar{\alpha}_1\right) \\ -\bar{n}_2\sin\bar{\alpha}_2 & \bar{n}_2\cos\bar{\alpha}_2 & \bar{n}_2\left(\Delta_{x,2}\cos\bar{\alpha}_2 + \Delta_{y,2}\sin\bar{\alpha}_2\right) \end{bmatrix} \begin{bmatrix} n_1 \\ n_2 \\ \alpha_1 \\ \alpha_2 \end{bmatrix}, \tag{3.37}$$

and the differential (asynchronous) control signal

$$\tilde{\tau}_{act} = \begin{bmatrix} \cos\overline{\alpha_1} & \sin\overline{\alpha_1} & \Delta_{x,1}\sin\overline{\alpha_1} - \Delta_{y,1}\cos\overline{\alpha_1} \\ \cos\overline{\alpha_2} & \sin\overline{\alpha_2} & \Delta_{x,2}\sin\overline{\alpha_2} - \Delta_{y,2}\cos\overline{\alpha_2} \\ -\overline{n_1}\sin\overline{\alpha_1} & \overline{n_1}\cos\overline{\alpha_1} & \overline{n_1}\left(\Delta_{x,1}\cos\overline{\alpha_1} + \Delta_{y,1}\sin\overline{\alpha_1}\right) \\ -\overline{n_2}\sin\overline{\alpha_2} & \overline{n_2}\cos\overline{\alpha_2} & \overline{n_2}\left(\Delta_{x,2}\cos\overline{\alpha_2} + \Delta_{y,2}\sin\overline{\alpha_2}\right) \end{bmatrix}. \quad (3.38)$$

Using such linearization, it is possible to describe the functions of independent changes in the rotation speed and angles of the AT motors.

3.3 ITERATIVE MATCHING OF THE SELECTED POSITION POINT WITH THE MOTION CONTROLLER LINEARIZATION FUNCTION

Since for a simplified model some position points give the best results depending on the expected vehicle maneuver, the simplified trigonometric function of the AT motor orientation is an important aspect when choosing the position point, since they are periodic. After linearization, the trigonometric function loses its characteristic behavior, and a higher value always leads to an increase in torque. Therefore, the obtained simulation behavior should correspond to the position point i in order to obtain the most realistic result. For a sharp turn of the ship, a non-zero value of α for the selected algorithm would be reasonable, and for a sharp change of trajectory, a higher value of n and a zero value of α would be reasonable. These two different approaches will be used for linearization and are described as follows, starting with the algorithm for a sharp change of the ship trajectory (ascending algorithm)

$$\alpha = \begin{bmatrix} 20 \\ 0 \end{bmatrix}. \quad (3.39)$$

Using this position point and substituting the values of Δx_i, and Δy_i, of both motors into (3.33) let's obtain

$$\tilde{\tau}_{act} = \begin{bmatrix} 2 & 0 \\ 0 & 40 \\ 0 & -16 \end{bmatrix} \begin{bmatrix} n \\ \alpha \end{bmatrix}. \quad (3.40)$$

For the ship turning algorithm, the position point is defined as follows

$$\alpha = \begin{bmatrix} 10 \\ \pi/6 \end{bmatrix}, \quad (3.41)$$

adjusted to correspond to the non-zero angle of the AT propellers. The turning speed has also decreased. Inserting this value of $\Delta_{x,i}$ and $\Delta y_{,i}$ into (3.33) let's obtain

$$\tilde{\tau}_{act} = \begin{bmatrix} \sqrt{3} & 10 \\ -1 & 10\sqrt{3} \\ 0.4 & -4\sqrt{3} \end{bmatrix} \begin{bmatrix} n \\ \alpha \end{bmatrix}. \tag{3.42}$$

These will be two different linearizations that will be used during the simulation. Theoretically, the latter should give better results when modeling with an increased search speed. Let's obtain two position:

$$\alpha_d = \begin{bmatrix} 20\ 20\ 0\ 0 \end{bmatrix}^T, \tag{3.43}$$

$$\alpha_d = \begin{bmatrix} 10\ 10\ -\pi/6\ -\pi/6 \end{bmatrix}^T, \tag{3.44}$$

which will also be used for differential linearization and have equivalent values. These position determination points define the following equations:

$$\tilde{\tau}_{act} = \begin{bmatrix} 1 & 1 & 0 & 0 \\ 0 & 0 & 20 & 20 \\ -0.1 & 0.1 & -8 & -8 \end{bmatrix} \begin{bmatrix} n_1 \\ n_2 \\ \alpha_1 \\ \alpha_2 \end{bmatrix}, \tag{3.45}$$

$$\tilde{\tau}_{act} = \begin{bmatrix} \frac{\sqrt{3}}{2} & \frac{\sqrt{3}}{2} & 5 & 5 \\ -\frac{1}{2} & -\frac{1}{2} & 5\sqrt{3} & 5\sqrt{3} \\ \frac{4-\sqrt{3}}{20} & \frac{\sqrt{3}+4}{20} & \frac{1+4\sqrt{3}}{2} & \frac{1-4\sqrt{3}}{2} \end{bmatrix} \begin{bmatrix} n_1 \\ n_2 \\ \alpha_1 \\ \alpha_2 \end{bmatrix}. \tag{3.46}$$

Such linearization can increase the ship maneuverability and create different approaches to solving the control problem.

3.4 ADAPTATION OF DEFINED STATE SPACES ACCORDING TO THE ALGORITHMIZATION OF THE CONTROLLER OPERATION

To use LQR, the model must be defined in the state space form:

$$\dot{x} = Ax + Bu, \tag{3.47}$$

$$y = Cx + Du, \tag{3.48}$$

where x – the controlled states; u – the input signals; y – the output signals; A – the state matrix; B – the input matrix; C – the output matrix; D – the forward coupling matrix. Therefore, if M_{RB} is the inverse matrix, (3.4) must be written as

$$\dot{\nu} = M_{RB}^{-1}\left(-L(\nu) - D(\nu)\nu + \tau_{act}\right). \tag{3.49}$$

Using this equation and substituting the parameters and variables from (3.6), (3.8) and (3.26), it is possible to simplify the equation for τ_{act}. τ_{act} will be replaced by $\tilde{\tau}_{act}$, which is one of the linearized parameters. The equation can be simplified as follows:

$$\dot{\nu} = \begin{bmatrix} \dot{u} \\ \dot{\nu} \\ \dot{r} \end{bmatrix} = \begin{bmatrix} \frac{mx^2 - I_Z}{m^2x_G^2 + m^2y_G^2 - I_Z m} & \frac{x_G y_G}{m^2x_G^2 + m^2y_G^2 - I_Z} & \frac{-y_G}{m^2x_G^2 + m^2y_G^2 - I_Z} \\ \frac{x_G y_G}{mx_G^2 + my_G^2 - I_Z} & \frac{my_G^2 - I_Z}{m^2x_G^2 + m^2y_G^2 - I_Z} & \frac{x_G}{mx_G^2 + my_G^2 - I_Z} \\ \frac{-y_G}{mx_G^2 + my_G^2 - I_Z} & \frac{x_G}{mx_G^2 + my_G^2 - I_Z} & \frac{-1}{mx_G^2 + my_G^2 - I_Z} \end{bmatrix}$$

$$\left(-\begin{bmatrix} 0 & 0 & 0 \\ 0 & 0 & m \\ 0 & 0 & mx_G \end{bmatrix} \begin{bmatrix} u \\ \nu \\ r \end{bmatrix} - \begin{bmatrix} X_u u & 0 & 0 \\ 0 & Y_\nu \nu & 0 \\ 0 & 0 & N_r r \end{bmatrix} + \mu\tilde{\tau}_{act} \right) =$$

$$= \left(\frac{1}{mx_G^2 + my_G^2 - I_Z} \right) \begin{bmatrix} \frac{mx_G^2 - I_Z}{m} & x_G y_G & -y_G \\ x_G y_G & \frac{my_G^2 - I_Z}{m} & x_G \\ -y_G & x_G & -1 \end{bmatrix} \mu\tilde{\tau}_{act} -$$

$$- \begin{bmatrix} \frac{x_u\left(mx_G^2 - I_Z\right)}{m} & Y_\nu x_G y_G & -N_r y_G \\ X_u x_G y_G & Y_\nu\left(mx_G^2 - I_Z\right) & N_r x_G - mx_G^2 - my_G^2 + I_Z \\ -X_u y_G & Y_\nu x_G & -N_r \end{bmatrix} \begin{bmatrix} u \\ \nu \\ r \end{bmatrix}. \tag{3.50}$$

Assuming that the value is sufficiently small, it can be approximated to 0. Then the equation for ν can be simplified even further

$$\dot{\nu} = \begin{bmatrix} -\frac{X_u}{m} & 0 & 0 \\ 0 & -\frac{Y_u}{m} & 1 \\ 0 & 0 & -\frac{N_r}{I_Z} \end{bmatrix} \begin{bmatrix} u \\ \nu \\ r \end{bmatrix} + \begin{bmatrix} -\frac{\mu}{m} & 0 & 0 \\ 0 & -\frac{\mu}{m} & 1 \\ 0 & 0 & -\frac{\mu}{I_Z} \end{bmatrix} \tau_{act}. \quad (3.51)$$

The resulting form can be viewed as a state space representation, where:

$$x = \nu, \quad (3.52)$$

$$A = \begin{bmatrix} -\frac{X_u}{m} & 0 & 0 \\ 0 & -\frac{Y_u}{m} & 1 \\ 0 & 0 & -\frac{N_r}{I_Z} \end{bmatrix}, \quad (3.53)$$

$$u = \begin{bmatrix} n \\ \alpha \end{bmatrix}, \quad (3.54)$$

$$B = \begin{bmatrix} -\frac{\mu}{m} & 0 & 0 \\ 0 & -\frac{\mu}{m} & 1 \\ 0 & 0 & -\frac{\mu}{I_Z} \end{bmatrix} \tau_{act}. \quad (3.55)$$

This is because the sensors used to determine the ship's position and speed are in a moving coordinate system, which leads to the following definitions:

$$y = \begin{bmatrix} u \\ \nu \\ r \end{bmatrix}, \quad (3.56)$$

$$C = \begin{bmatrix} 1 & 0 & 0 \\ 0 & 1 & 0 \\ 0 & 0 & 1 \end{bmatrix}, \quad (3.57)$$

$$D = \begin{bmatrix} 0 & 0 \\ 0 & 0 \\ 0 & 0 \end{bmatrix}. \tag{3.58}$$

B will vary depending on the linearization of the input signal used, for example, if (3.40) and (3.42) are used. From (3.3) and (3.5), these values can be transferred to the *n*-system, where it is assumed that $\psi = 0$.

3.5 STRUCTURING A LINEAR QUADRATIC REGULATOR (LQR) AS A LINEARIZATION OBJECT

The main goal of the problem of adequate ship control is to minimize the design criterion, i.e., to balance it between the magnitude of the tracking error $e = y - r$ and the magnitude of the input signal. Sometimes such a paradigm can be viewed as an optimization problem, when the system is described by a linear differential equation, and the integration relationships are described by quadratic functions. Then the goal is to find the control law $u = -L_x$, where:

$$L = \arg\min \int_0^\infty \left(z^T(t) Q_1 z(t) + u^T(t) Q_2 u(t) \right) dt, \tag{3.59}$$

$$u = -Lx, \tag{3.60}$$

where Q_1 and Q_2 — weight matrices that can be used as design variables for this resulting controller. The optimization problem is solved using the expression

$$L = Q_2^{-1} B^T S, \tag{3.61}$$

where S — a positive semidefinite matrix that solves the Riccati algebra equation

$$A^T S + SA + M^2 Q_1 M - SBQ_2^{-1} B^T S = 0. \tag{3.62}$$

This equation can be solved using software such as MatLab/Simulink.

To achieve the desired design behavior of the system, an iterative modeling process and adjustment according to the observed controller behavior are required to find the optimal value of the constant coefficients. The controller defined above resets the system state to zero, but in this case the controller must follow a given reference signal.

Therefore, it is necessary to integrate the reference signal r in the equations. This can be done by rewriting the input signal as

$$u(t) = -Lx(t) + L_r r(t), \tag{4.63}$$

where L_r is chosen so that the static gain corresponds to the given value. A similar method of using LQR was applied in [29]. The system developed according to the above principle is shown in **Fig. 3.4**.

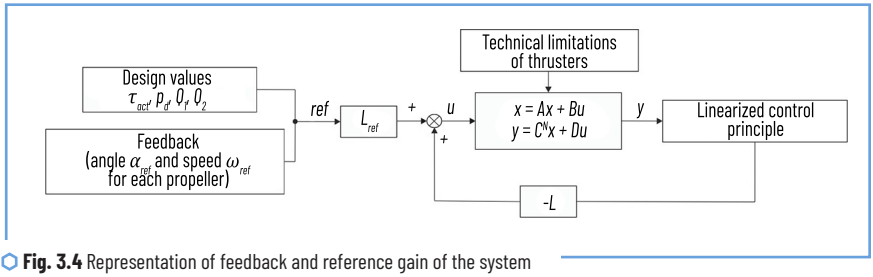

Fig. 3.4 Representation of feedback and reference gain of the system

Every system has uncertainties. Usually these uncertainties are modeled as a random stochastic process ("white noise"), which is a random signal with a constant spectrum. Taking into account the uncertainty, the model can be written as:

$$\dot{x} = Ax + Bu + Nv_1, \tag{3.64}$$

$$z = Mx, \tag{3.65}$$

$$y = Cx + v_2, \tag{3.66}$$

where v_1 and v_2 – white Gaussian noise with zero mean. In order to filter these signals, a state observer can be implemented that uses an estimate of the following form

$$\hat{x} = A\hat{x} = Bu + K(y - C\hat{x}) = (A - KC)\hat{x} + Bu + Ky. \tag{3.67}$$

This problem can be solved by describing it as an optimization problem by analogy with the definition of LQR with minimization of the variance of the estimation error. The estimation error can be denoted as $e = x - \hat{x}$, then the variance will be equal to $E_e(t)e(t)$. If v_1 and v_2 are independent and have zero mean, it is possible to assume that:

$$Ev_1v_1^T = R_1, \tag{3.68}$$

$$Ev_2v_2^T = R_2, \tag{3.69}$$

$$Ev_1v_2^T = 0. \tag{3.70}$$

Then the state observer can be described as:

$$K = PCR_2^{-1}, \tag{3.71}$$

where P — the covariance of the optimal estimator that solves the Riccati equation

$$A^T P + PA + NR_1 N^T - PC^T R_2^{-1} CP = 0. \tag{3.72}$$

The Kalman gain can also be found using Matlab/Simulink. Equation (3.72) is called the Kalman filter, where R_1 and R_2 are design variables and can be tuned to filter out process and measurement disturbances. LQR methods and Kalman filtering are discussed in detail in. The combined use of Kalman filtering and LQR is called Linear-Quadratic-Gaussian control (LQG). Similar approaches to using similar methods to solve such problems are discussed in [30].

MONITORING SYSTEM STRUCTURE

To predict the controller states, it is necessary to use a monitoring system using sensors used in marine navigation. The main monitoring systems used in ship control are the Inertial Measurement Unit (IMU) and the Global Positioning System (GPS).

STRUCTURE OF THE INERTIAL MEASUREMENT UNIT

The IMU uses a combination of accelerometers, gyroscopes, and magnetometers to measure angular speeds, accelerations, and magnetic fields. It is an important device for ship control because ships can move and rotate in all 6 degrees of freedom. The measurements from the gyroscope and accelerometer include some biases that create a systematic measurement error. If the angular speeds and accelerations are integrated, the resulting linear speed errors will increase linearly with time, and the orientation error will increase quadratically. Therefore, it will be difficult to rely solely on the IMU for this purpose over a longer period of time [31].

GLOBAL POSITIONING SYSTEM STRUCTURE WITH SENSOR INTEGRATION FOR CONDITION DETECTION

GPS is a system that uses satellite communication and data exchange with a receiver and provides location and time information in areas with unobstructed direct visibility. The most common GPS has for autonomous vehicles, the development and implementation of a high-integrity navigation system is based on the combined use of GPS and IMU. Improving the integrity of the navigation cycle will be carried out by

detecting possible faults both before and during the synthesis process. The implementation of this fault detection methodology takes into account both low-frequency faults in the IMU caused by sensor drift and device displacement, and high-frequency faults in the GPS receiver caused by multipath errors.

Using a Kalman filter to combine the information provided by the two sensors, it is possible to reduce the negative effects. The IMU offset can be adjusted, and when the GPS sensor is not in line of sight, the controller will rely more heavily on the IMU until the GPS is back in line of sight [32, 33]. However, since most maritime routes pass through open sky areas, the GPS signal will always be present, and therefore the main focus will be on correcting the IMU offset. This type of sensor integration for open air vehicle control is used where land-based vehicles are used instead of the SBV.

3.6 PHYSICAL MODELING OF A MARINE-BASED VEHICLE

The SBV physical scale model based on a controller that uses inputs from the GPS and IMU to determine the ship's position, heading, and speed.

Based on this data, the controller will control the actuators, the Electronically Commutated Motor (ECM), and the servo for each AT. The ECM are connected to the AT screw through gear transmissions (**Fig. 3.5**). The gear ratio between the servo drive and the AT connection is quite large. The main characteristics of the AT formalized physical model are presented in **Fig. 3.6** [34, 35].

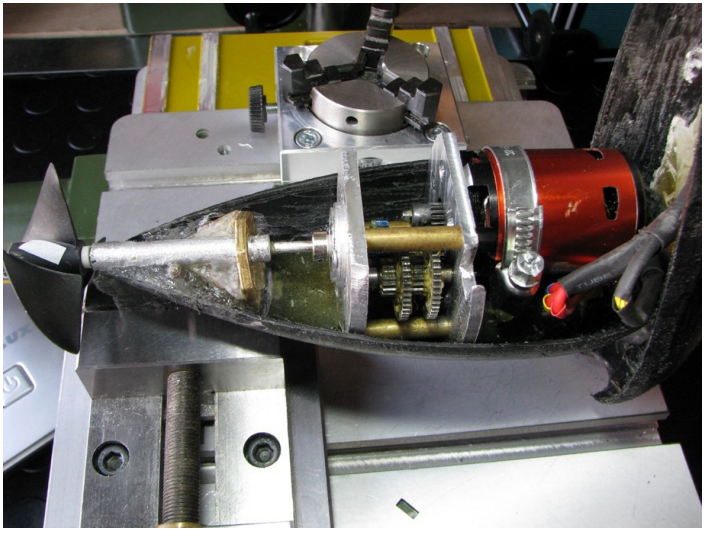

Fig. 3.5 Gearbox connecting the ECM to the AT screw

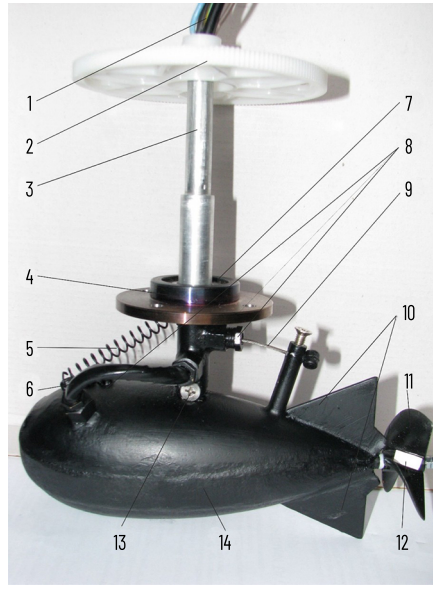

Fig. 3.6 Physical model of the thruster with two degrees of freedom: 1 — ECM power cable and the cable of the drive of changing the angle of inclination; 2 — driving gear of the baller rotation drive; 3 — baller; 4 — bearing shield; 5 — feedback spring of the drive of changing the angle of inclination; 6 — power cable; 7 — support bearing; 8 — gland entries; 9 — cable of the drive of changing the angle of inclination; 10 — stabilizing wings; 11 — GFK; 12 — luminescent tag for remote measurement of the frequency of GFK rotation; 13 — connection point of the baller with the AT body; 14 — AT body with the AT ECM located in the middle

To control the speed and torque of the ECM, the motor currents are measured and the throughput is calculated with high accuracy (**Fig. 3.7, 3.8**). Torque control is an integral part of the design of most applied speed control circuits of AT electric drive systems.

Theoretically, the torque rise time in a frequency converter (FC) with pulse-width modulation (PWM) is limited by the motor inductance in dependent current inverters with a DC link [36].

However, in practice, the controller limits the rate of change of torque to prevent damage to the mechanical part of the electric drive.

Thus, the transfer function of the controller can be described by the dependence [37]:

$$F_p(S) = \frac{1}{\left(1 - t_{FC} S\right)} M_d(s), \tag{3.73}$$

where t_{FC} = 20÷200 ms.

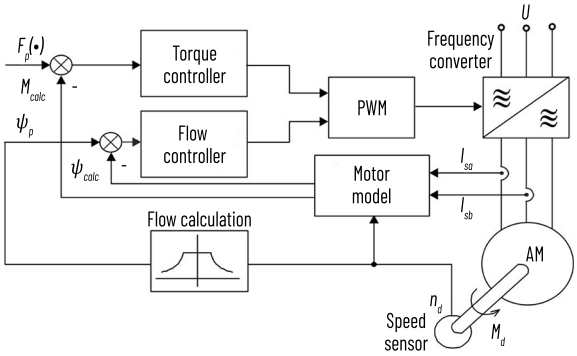

Fig. 3.7 Block diagram of the AT ECM closed-loop torque control system: Ψ_p and Ψ_{calc} — the values of the set and calculated fluxes, I_{sa}, I_{sb} — the measured values of the stator currents

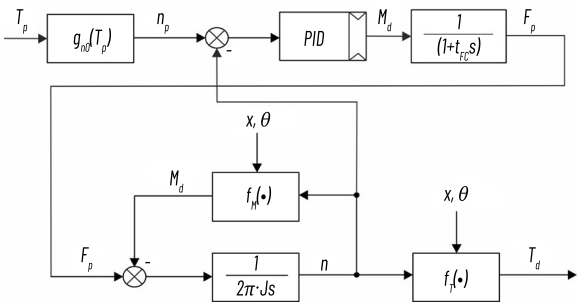

Fig. 3.8 Block diagram of the ECM speed controller

3.7 SIMULATION STUDIES OF THE CHANGE IN THE YAW SPEED BASED ON THE DEFINED STATE SPACE

To investigate the behavior of the physical scale model of the ship during a turn, a setting step is made at the reference yaw speed. To check the possibilities and realistic implementation in practice, two different simulations are performed: one in which there is some "softening" of the settling time and overshoot occurs (peak test), and the other in which the controller tries to adhere to the reference setting as "rigidly" as possible (smooth test). The peak test was adjusted so that all simulations, including this one, had the same settling time of approximately 10 seconds after the start of the setting. Since linearization and simplification of the model were performed, this test may give unrealistic results, but, as before, it is considered to be consistent with the capabilities of the control system [38].

DETERMINATION OF THE ERROR OF SYNCHRONOUS CONTROL WITH ZERO THRUSTER ANGLE FROM THE SELECTED POSITION MATRIX

For the following simulations, the same rotational speed and propeller angle are chosen for both APUs.

In this simulation, the controller uses matrices obtained by linearizing around the operating point with translational motion of the input signals (3.40), which are designed to operate with propeller angles close to zero. Two different settings are used for the controller, which are performed for two objectives: first, for the condition when the input signals are equal to 1, and the reference gain is adjusted to achieve the target value. Another setting eliminates the tracking error for increasing the rotation speed, providing the closest to the reference speed value, while maintaining the input signal level for the lower swing speed value. Therefore, finding the setting limit takes more time, which provides information about the system capability by comparing the evenly and more aggressively tuned system. The matrices of reference coefficients and transfer coefficients, where p and s denote the peak and smoothing indices, respectively, will look like [39]:

$$Q_{1,p} = \begin{bmatrix} 1 & 0 & 0 \\ 0 & 1 & 0 \\ 0 & 0 & 1 \end{bmatrix}, Q_{1,s} = \begin{bmatrix} 1 & 0 & 0 \\ 0 & 0.001 & 0 \\ 0 & 0 & 200 \end{bmatrix},$$

$$Q_{2,p} = \begin{bmatrix} 1 & 0 \\ 0 & 1 \end{bmatrix}, Q_{2,s} = \begin{bmatrix} 1 & 0 \\ 0 & 1 \end{bmatrix},$$

$$L_{r,p} = \begin{bmatrix} 0 & 0 & 1 \\ 0 & 0 & -22.14 \end{bmatrix}, L_{r,s} = \begin{bmatrix} 0 & 0 & 1 \\ 0 & 0 & -14.06 \end{bmatrix}. \quad (3.74)$$

Fig. 3.9 shows the main results of the operation of two different controllers. The maximum value controller provides an overshoot of 7 times the reference value, but stabilizes after 10 s.

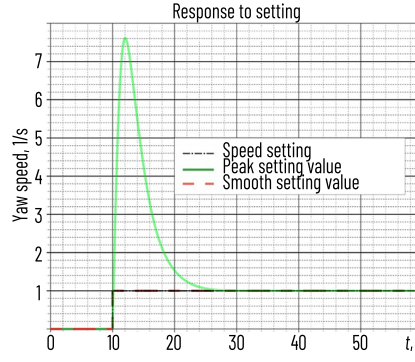

Fig. 3.9 Transient characteristic of zero angle linearization

According to **Fig. 3.10, *b***, the final value of α is $\alpha_p = \alpha_s = 0.065$ rad.

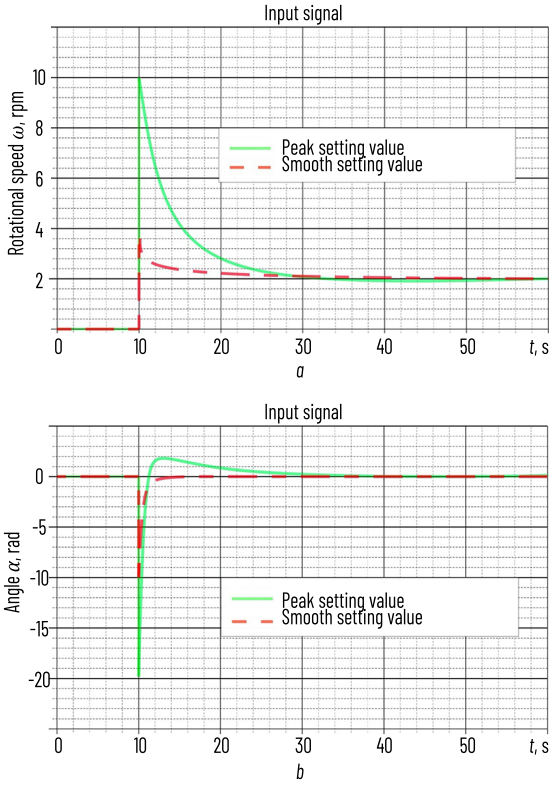

Fig. 3.10 Input signals of zero angle linearization: *a* — rotation speed; *b* — angle α

This is most likely the result of changing the AT angle, as shown in **Fig. 3.10, *a, b***, where α reaches a very high negative value, close to — 20 rad, which is far from the realistic scenario for a real AT.

This fact gives grounds to reassess the need for a more drastic change in the crawl speed over the slow one to counteract the condition when the overshoot reaches such a high value. However, decreasing α is physically reasonable, because a small negative angle will provide a positive torque around the *z*-axis and a positive crawl speed. Although it may be debatable if such a small angle can have such an effect, if a zero angle gives similar results for this controller mode. Another interesting aspect is how separated the rotation

speed and the speed jumps are, since the controller shows the same behavior for both simulations, which for a real AT can significantly affect the results [40].

In a smooth controller, the output value seems to "follow" the reference value, but has two differences from the other controller: the same decrease and restoration of α to the final stabilized value in less than a second, which is not possible for a real AT due to its dynamic properties. In **Fig. 3.11**, the oscillation speed is set much slower, which may indicate that there is some uncoupled behavior, since the input signal to the system is the same time interval of 20 seconds, but the oscillation speed at this time is different. Some unrealistic AT behavior may be associated with the linearization of α and its trigonometric dependence. The trigonometric function, which is periodic and only distributes the forces created by the number of revolutions between the x_b and y_b axes, cannot exceed 1. When applying linearization, the controller "believes" that a higher value of α corresponds to a higher value of the resulting force, which in practice is not true.

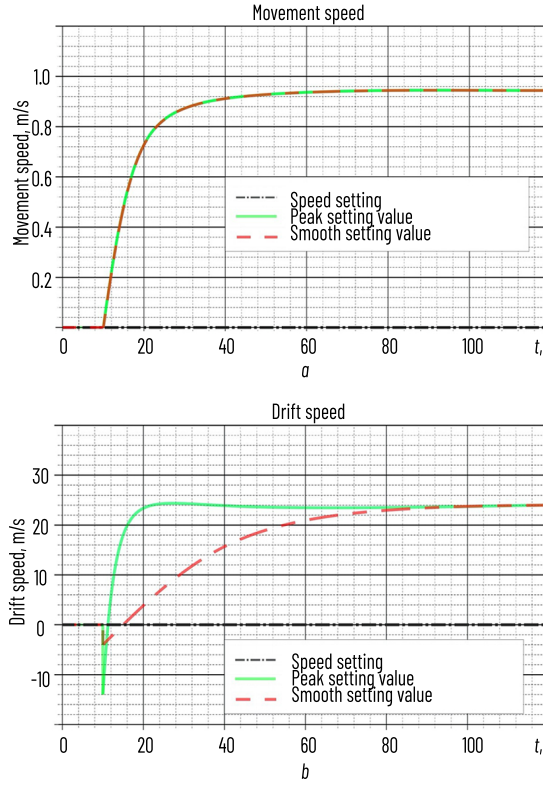

Fig. 3.11 Linearization at zero angle: *a* — speed; *b* — drift speed

DETERMINATION OF THE ERROR OF SYNCHRONOUS CONTROL WITH A NON-ZERO ANGLE OF THE THRUSTERS BY THE SELECTED LOCATION MATRIX

The model is tuned based on the linearization method (3.41), where the angle of the propellers α has a small negative value, which is considered close to the resulting final value for a given simulation of the yaw speed. This is done in order to see if this tuning will give better results than linearization with a zero angle. The design goals of the tuning are similar to the previous simulations. One of the main differences is that the third element in the first row for a given gain value also needed tuning, otherwise the speed jump tends to take a negative value, which requires a different behavior of the model and makes it difficult to compare the two simulations. The weight matrices and gain values for this simulation are as follows:

$$Q_{1,p} = \begin{bmatrix} 1 & 0 & 0 \\ 0 & 1 & 0 \\ 0 & 0 & 1 \end{bmatrix}, Q_{1,s} = \begin{bmatrix} 1 & 0 & 0 \\ 0 & 0.001 & 0 \\ 0 & 0 & 225 \end{bmatrix},$$
$$Q_{2,p} = \begin{bmatrix} 1 & 0 \\ 0 & 1 \end{bmatrix}, Q_{2,s} = \begin{bmatrix} 1 & 0 \\ 0 & 1 \end{bmatrix},$$
$$L_{r,p} = \begin{bmatrix} 0 & 0 & 10 \\ 0 & 0 & -21.6 \end{bmatrix}, L_{r,s} = \begin{bmatrix} 0 & 0 & 3.63 \\ 0 & 0 & -14.09 \end{bmatrix}. \quad (3.75)$$

which gives the results shown in **Fig. 3.12–3.14**.

According to **Fig. 3.13**, the final value of α is: $\alpha_p = \alpha_s = 0.0168$ rad.

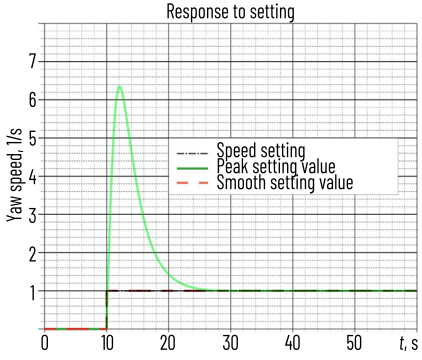

Fig. 3.12 Transient response with non-zero angle α

These results are similar to those obtained but with some differences in the behavior of the model. The peak tuning gives slightly better results, since its overshoot reaches only 6 times the reference value.

The main difference is the higher propeller speed, which is almost ten times more influential on the longitudinal speed. That is, the non-minimum phase response coincides with the fastest response when the maximum peak speed of the setting is reached. The smooth tuning makes the controller response slower than during the "peak tuning" according to $Q_{1,s}$ (3.75).

The most interesting thing in this simulation compared is the input signal graphs in **Fig. 3.13, *a*, *b***. The rotation speed has a much larger value, unlike the angle α, the resulting transient response of which has almost not changed. First, this may be the result of linearization, in which the controller mainly responds to the angle α setting with n maintained at the same level, if there is no need to increase the rotation speed. Second, the input signals show which setpoint values for α are positive, close to zero, but positive. Theoretically, for the simulation process, this should not be the case.

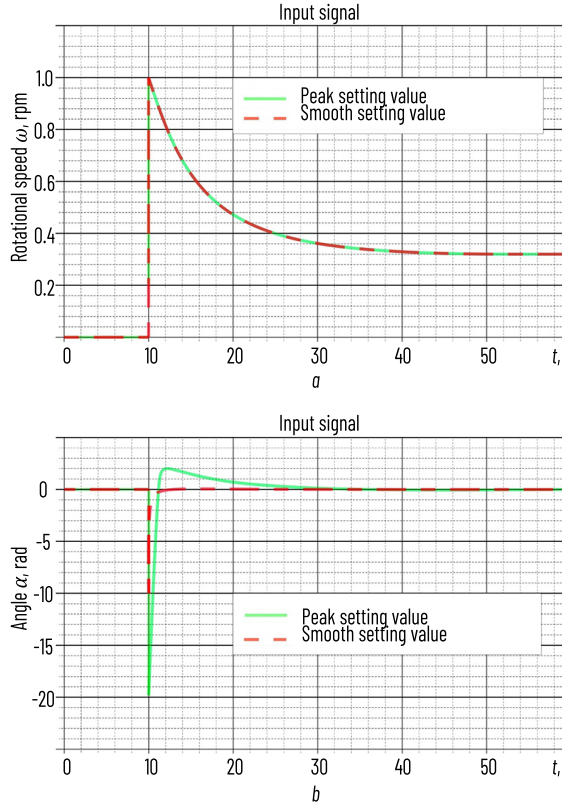

Fig. 3.13 Input signals with non-zero angle α: *a* — propeller rotation frequency; *b* — angle α

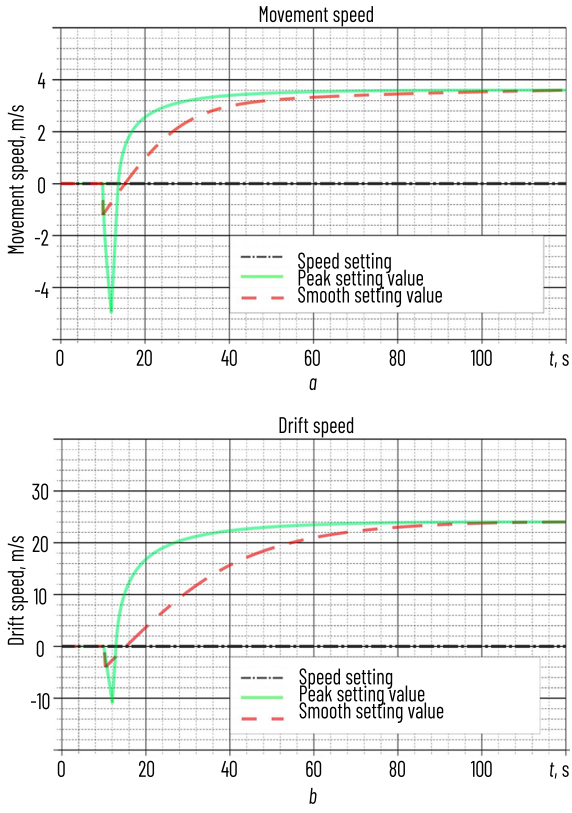

Fig. 3.14 Dependences of speeds with non-zero angle α: *a* — speed of movement; *b* — drift speed

DETERMINATION OF THE ERROR OF ASYNCHRONOUS CONTROL WITH ZERO ANGLE OF THRUSTERS BY THE SELECTED LOCATION MATRIX

The following simulation uses differential control, in other words, the possibility of independent control of the speed and angle of rotation of both ATs.

First, linearization with zero angle α is used for differential (asynchronous) control of the stern ATs. The simulation is carried out according to the same algorithm to study two tuning schemes with different goals. Using differential (asynchronous) control, one can observe a slightly different, potentially more improved behavior of the controller, which is confirmed by the following results:

$$Q_{1,p} = \begin{bmatrix} 1 & 0 & 0 \\ 0 & 1 & 0 \\ 0 & 0 & 1 \end{bmatrix}, Q_{1,s} = \begin{bmatrix} 1 & 0 & 0 \\ 0 & 0.015 & 0 \\ 0 & 0 & 270 \end{bmatrix},$$

$$Q_{2,p} = \begin{bmatrix} 1 & 0 & 0 & 0 \\ 0 & 1 & 0 & 0 \\ 0 & 0 & 1 & 0 \\ 0 & 0 & 0 & 1 \end{bmatrix}, Q_{2,s} = \begin{bmatrix} 1 & 0 & 0 & 0 \\ 0 & 1 & 0 & 0 \\ 0 & 0 & 1 & 0 \\ 0 & 0 & 0 & 1 \end{bmatrix},$$

$$L_{r,p} = \begin{bmatrix} 0 & 0 & 1 \\ 0 & 0 & 1 \\ 0 & 0 & -20 \\ 0 & 0 & -20 \end{bmatrix}, L_{r,s} = \begin{bmatrix} 0 & 0 & 1 \\ 0 & 0 & 1 \\ 0 & 0 & -12.32 \\ 0 & 0 & -12.32 \end{bmatrix}. \quad (3.76)$$

The final values of α_p and α_s (**Fig. 3.15**) are: $\alpha_p = -0.084$ rad, $\alpha_s = -0.41$ rad.

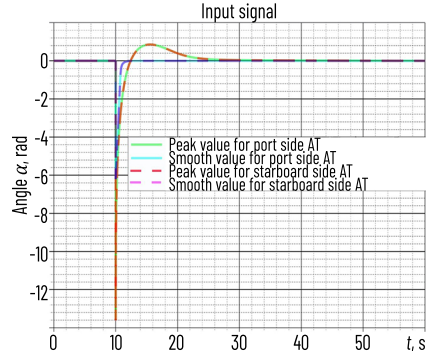

Fig. 3.15 Differential input signals at a given zero angle α

The transient responses for the longitudinal, drift and yaw speeds (**Fig. 3.16** and **3.17**) show the AT operation similar to the synchronous control simulation. Here the step response is lower and the longitudinal speed reaches a higher final value. However, some interesting things can be observed in the input signals. The angle α is the same for both motors with two different settings, despite the AT having differential degrees of freedom. This may be the result of linearization, which makes it the only adequate solution. The large dip shown in **Fig. 17, *b*,** with the simulation is smaller, indicating steps in the right direction. The final value of α for the peak setting is almost the same as for the synchronous control, but the smooth setting is closer to the actual value of $\pi/6$, which is also a good indicator for this controller.

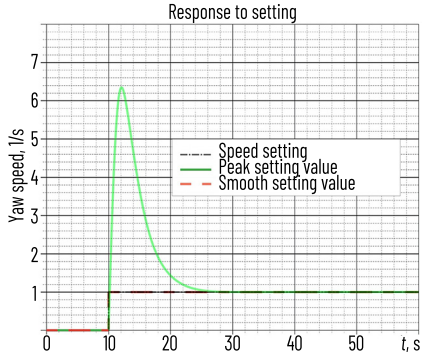

Fig. 3.16 Differential transient response for zero angle α

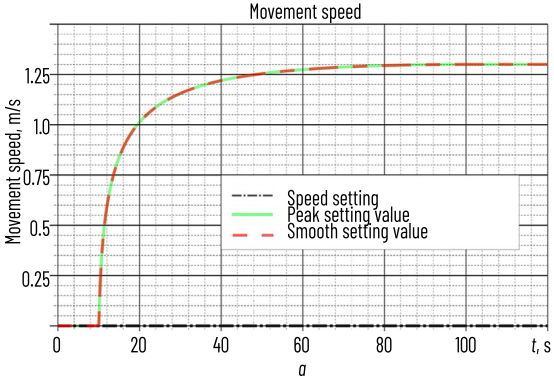

a

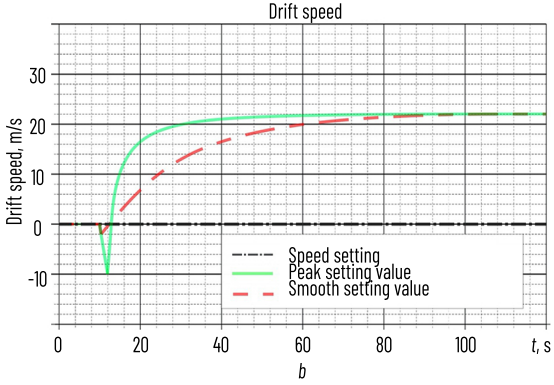

b

Fig. 3.17 Differential speeds at zero angle α: *a* – longitudinal motion; *b* – drift

It is possible to observe completely different indicators n (**Fig. 3.18**), which indicates a smaller influence on the system of this input signal. For both settings, one of the screws rotates at a lower speed, which in practice is an advantage. When one motor provides more thrust, it creates a corresponding torque, turning the ship.

Using this difference in rotation speed, the controller can more effectively regulate the speed of the ship's turn.

The problem that can be seen in this simulation is that any configuration of the values of the AT rotation speed moves the ship "wrongly".

Since motor 1 is located to the right of the x_b axis, and motor 2 to the left, such a run will provide a negative speed of turn.

This is another sign that the controller is counteracting itself, which confirms the consequence of the linearization of the input signal.

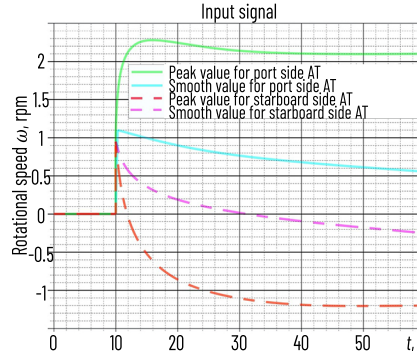

Fig. 3.18 Differential speeds of rotation of the APU at zero angle α

DETERMINATION OF THE ASYNCHRONOUS CONTROL ERROR WITH A NON-ZERO ANGLE OF THE THRUSTERS BY THE SELECTED LOCATION MATRIX

The following settings are based on the model with linearization of the non-zero differential angle (3.41) and have the same tuning aspects as in the previous simulation with the same problem, where the controller required negative speed jumps.

Therefore, this was also corrected by tuning the controller. The weight matrices and the reference gain have the following form:

$$Q_{1,p} = \begin{bmatrix} 1 & 0 & 0 \\ 0 & 1 & 0 \\ 0 & 0 & 1 \end{bmatrix}, Q_{1,s} = \begin{bmatrix} 1 & 0 & 0 \\ 0 & 0.05 & 0 \\ 0 & 0 & 250 \end{bmatrix},$$

$$Q_{2,p} = \begin{bmatrix} 1 & 0 & 0 & 0 \\ 0 & 1 & 0 & 0 \\ 0 & 0 & 1 & 0 \\ 0 & 0 & 0 & 1 \end{bmatrix}, Q_{2,s} = \begin{bmatrix} 1 & 0 & 0 & 0 \\ 0 & 1 & 0 & 0 \\ 0 & 0 & 1 & 0 \\ 0 & 0 & 0 & 1 \end{bmatrix},$$

$$L_{r,p} = \begin{bmatrix} 0 & 0 & 5 \\ 0 & 0 & 5 \\ 0 & 0 & -5.31 \\ 0 & 0 & -5.31 \end{bmatrix}, L_{r,s} = \begin{bmatrix} 0 & 0 & 6 \\ 0 & 0 & 6 \\ 0 & 0 & -9.81 \\ 0 & 0 & -9.81 \end{bmatrix}. \quad (3.77)$$

The simulation results are presented in **Fig. 3.19–3.23**.

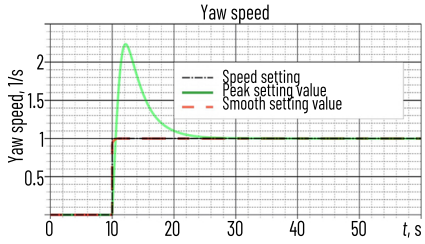

Fig. 3.19 Differential transient response with non-zero angle α

The final values of α_p and α_s (**Fig. 3.22**) are:

$\alpha_{p,1} = 3.64$ rad, $\alpha_{s,1} = 2.68$ rad;

$\alpha_{p,2} = -4.81$ rad, $\alpha_{s,2} = -3.52$ rad.

The simulation results are unique among all the search speed simulations. The peak step shows that the outlier is significantly lower than in any of the previous calculations. This overshoot only reaches twice the reference value. The transient plots in **Fig. 3.22** show similar results to the previous simulations, but with different final values. They can be adjusted by applying a reference gain, which is not necessary, since the goal of the simulation is to find out how the AT behavior affects the system, not what the final values of the angles α are.

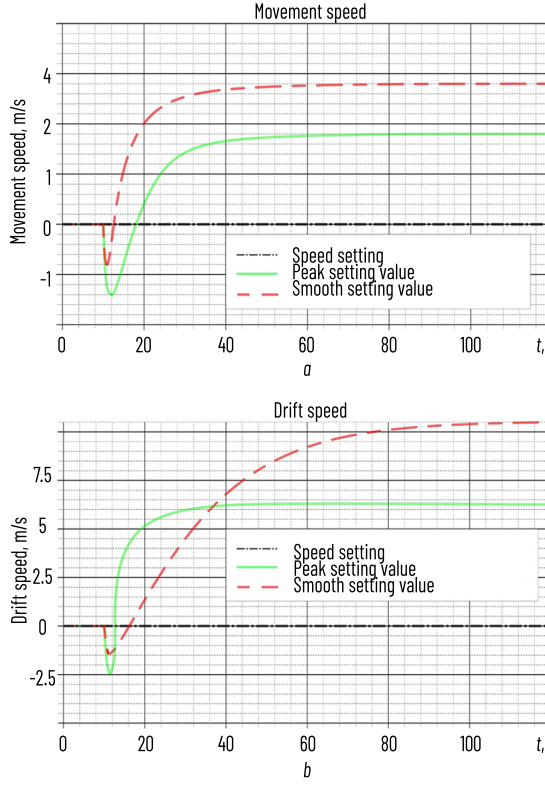

Fig. 3.20 Differential speeds at a non-zero angle α: *a* — longitudinal motion; *b* — drift

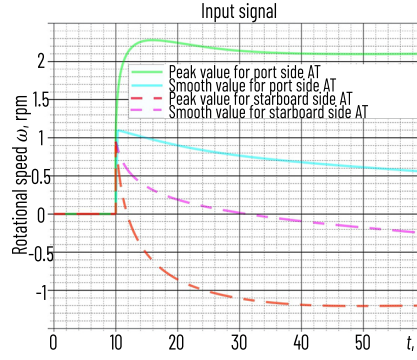

Fig. 3.21 Differential rotational speeds with a non-zero angle

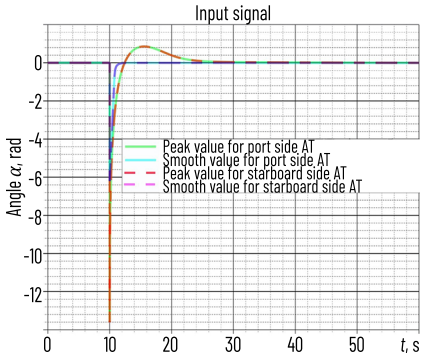

Fig. 3.22 Differential input signals at a given non-zero angle α

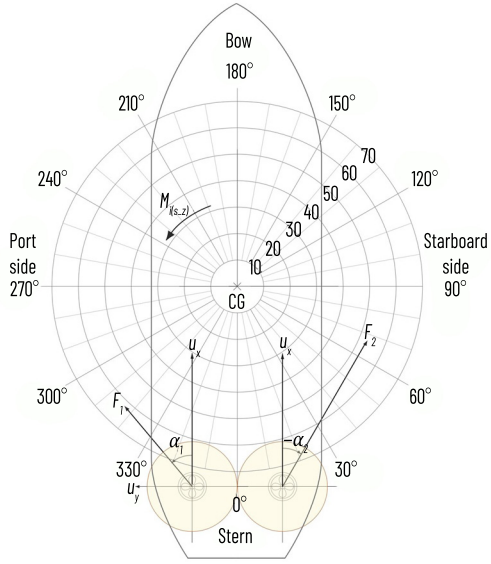

Fig. 3.23 Position and angle of rotation of motor *i*

However, in practice, the input signals "behave" realistically. Both the step and smooth tuning lead to similar transient characteristics, but with different final values. These values have been interpreted and illustrated in **Fig. 3.23**. Here it is possible to see that both AT motors, as in the previous simulations,

counteract each other, but now in a controlled manner. The left AT has a larger angle α compared to the right, which provides a larger torque about the z axis and, therefore, an increase in the turning speed. While the right motor has a higher rotation speed, creating a negative torque about the z axis and, thus, canceling the forces from the left motor. This allows to achieve a constant turning speed. However, the method creates many unnecessary opposing forces in the y_b direction. The angle values are still far from the operating point, which makes the linearization accuracy low. However, the obtained results show trends in the right direction.

DETERMINATION OF THE LIMITING CHARACTERISTICS OF THE CONTROLLER

To further test the capabilities of the system, a controller was developed to set the azimuthal angle limits instead of strictly following the reference sweep speed step. This simulation was performed with differential non-zero angle linearization. The weight and reference gain matrices for this simulation are as follows:

$$Q_1 = \begin{bmatrix} 0.01 & 0 & 0 \\ 0 & 0.01 & 0 \\ 0 & 0 & 1 \end{bmatrix}, Q_2 = \begin{bmatrix} 1 & 0 \\ 0 & 1 \end{bmatrix}, L_r = \begin{bmatrix} 0 & 0 & 6 \\ 0 & 0 & 6 \\ 0 & 0 & -1.31 \\ 0 & 0 & -1.31 \end{bmatrix}. \quad (3.78)$$

The simulation results are shown in **Fig. 3.24–3.27**.

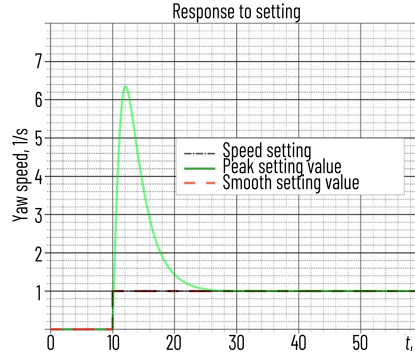

Fig. 3.24 Setting step characteristic limits

The final values of α_1 and α_2 (**Fig. 3.27**) are:

$\alpha_1 = 0.63$ rad, $\alpha_2 = -0.28$ rad.

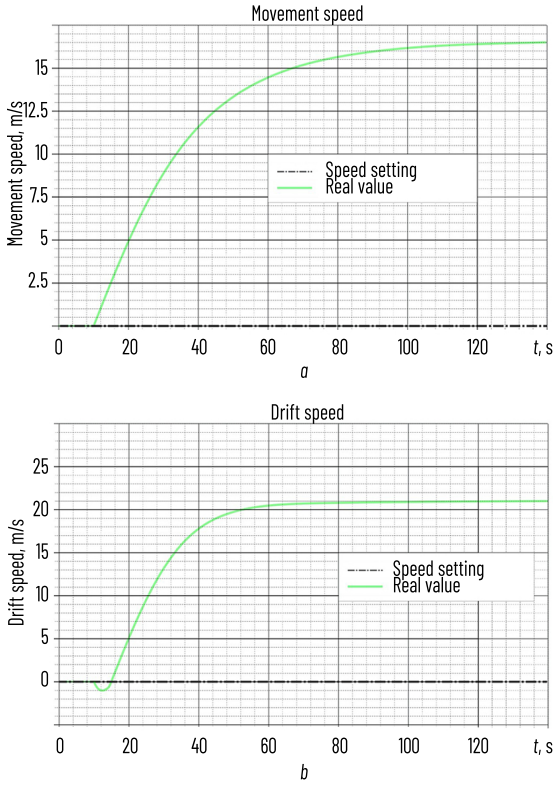

Fig. 3.25 Limit settings: *a* – longitudinal acceleration; *b* – drift acceleration

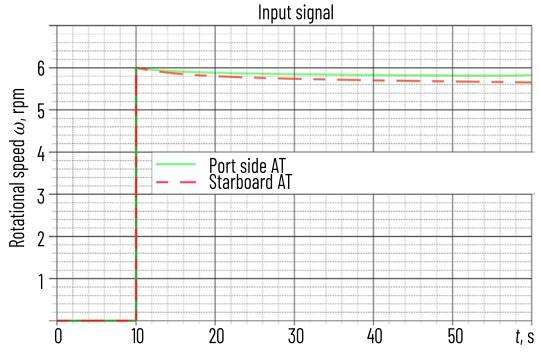

Fig. 3.26 Rotation speed limit settings

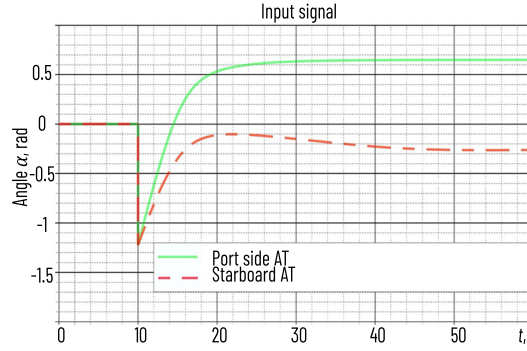

Fig. 3.27 Angle α limit settings

Table 3.1 shows the calculated data and parameters of the SBV physical model *0* (**Fig. 3.1, 3.5, 3.6**) for real-time modeling of the model behavior in the dynamic positioning mode with adequate distribution of the AT thrust and generation of optimal control input data.

Table 3.1 Parameters of the SBV model and thrusters

Name	Designation	Unit	Value
Port side AT	Δ_{yl}	m	–1.22
	Δ_{xl}	m	–0.23
	F_{max}	N	894
	F_{min}	N	0.264
	ω	rev/s	7.96
	α_{lmax}	Rad	3.925
	α_{lmin}	Rad	–0.785
	$\Delta\alpha$	Rad	0.088
	M_p (56)	m/(rev/s)^2	6.6e–4
Starboard AT	Δ_{x2}	M	0.23
	α_{2max}	rad	–0:175
	α_{2min}	rad	–3:054

The SBV model with the AT moved forward with a constant thrust force F_x, and changed course by turning the torque varying in time with a duration of 450 s. Random "noise" was added to the desired generalized force to check the reliability and stability of the given thrust distribution method.

CONCLUSIONS

Improvement of the AT linear-quadratic control method of the ship's propulsion complex consisted in determining the state spaces and linearizing the control system, which allowed to adequately model the ship's yaw rate and track the influence of disturbing forces on the controller characteristics. Moreover, it was found that small negative angles provide a positive torque around the z axis and a positive yaw rate. To take into account the dynamic properties of real AT, it is necessary to be able to regulate the reduction and restoration of the angle α to the final stabilized value. It can also be concluded that when applying linearization, a larger value of α corresponds to a larger value of the resulting force, which in practice does not correspond to reality.

Verification of the model behavior showed that in order to obtain a relatively adequate transient response with minimal overshoot, it is necessary to minimize the tracking error. Studies of the design features of ships of this class confirm that jumps in the speed of AT rotation, which are stabilized with a constant zero angle, lead to a quick response to the jump and the absence of overshoot. Small angles of the AT location relative to the diametrical plane of the ship lead to the fact that both AT motors require a lower speed of rotation to provide a given thrust.

For physical scale modeling, AT physical model in the stern can be implemented on the basis of actuators, an electronically commutated motor and a servo drive for each AT. The electronically commutated motor is connected to the AT propeller through gears. In practice, the controller uses input data from GPS and IMU to determine the position, course and speed of the ship. To regulate the speed and torque of the electric motor, it is necessary to measure the motor currents and calculate the bandwidth of the converters with high accuracy. In practice, it is necessary to provide a limit on the rate of change of torque to prevent damage to the mechanical part of the electric drive.

Independent control of the speed and angle of the AT with linearization with zero or non-zero angle of the AT has proven its greater controllability than synchronous. To reduce the resistance of the AT motors, it is necessary to apply a coordinated change in the angle α with the speed of rotation. And to compensate for the corresponding forces, it is necessary to adjust the speed of rotation, creating a negative torque around the z axis. Increasing the accuracy of linearization is possible by eliminating excess opposing forces in the y_b direction.

Using the predictive gain method in the future will allow, although reducing the versatility of the controller, to increase its realism. To improve the performance of the models, the controller was tuned to more realistic output and input parameters. Changing the principles of linearization of the input signal led to the fact that it acts more like a trigonometric function of predictive gain. The result allowed to clarify the influence of the AT orientation on the ship position, and the linearity of the model on the controller functionality.

REFERENCES

1. Budashko, V., Nikolskyi, V., Onishchenko, O., Khniunin, S. (2016). Decision support system's concept for design of combined propulsion complexes. Eastern-European Journal of Enterprise Technologies, 3 (8 (81)), 10–21. https://doi.org/10.15587/1729-4061.2016.72543

2. Budashko, V. V. (2017). Design of the three-level multicriterial strategy of hybrid marine power plant control for a combined propulsion complex. Electrical Engineering & Electromechanics, 2, 62–72. https://doi.org/10.20998/2074-272x.2017.2.10
3. Budashko, V. (2017). Formalization of design for physical model of the azimuth thruster with two degrees of freedom by computational fluid dynamics methods. Eastern-European Journal of Enterprise Technologies, 3 (7 (87)), 40–49. https://doi.org/10.15587/1729-4061.2017.101298
4. Budashko, V. V. (2016). Increasing control's efficiency for the ship's two-mass electric drive. Electrical Engineering & Electromechanics, 4, 34–42. https://doi.org/10.20998/2074-272x.2016.4.05
5. Budashko, V., Sandler, A., Khniunin, S. (2023). Improving the method of linear-quadratic control over a physical model of vessel with azimuthal thrusters. Eastern-European Journal of Enterprise Technologies, 1 (2 (121)), 49–71. https://doi.org/10.15587/1729-4061.2023.273934
6. Myrhorod-Karpova, V., Hvozdeva, I., Budashko, V. (2022). Multiparameter Approximation Model of Temperature Conditions of Marine Diesel Generator Sets, Based on Markov Chain Monte Carlo. TransNav, the International Journal on Marine Navigation and Safety of Sea Transportation, 16 (4), 779–784. https://doi.org/10.12716/1001.16.04.20
7. Budashko, V., Golikov, V. (2017). Theoretical-applied aspects of the composition of regression models for combined propulsion complexes based on data of experimental research. Eastern-European Journal of Enterprise Technologies, 4 (3 (88)), 11–20. https://doi.org/10.15587/1729-4061.2017.107244
8. Budashko, V., Sandler, A., Glazeva, O. (2024). Improvement of the Predictive Control Method for the High-Level Controller. 2024 IEEE 17th International Conference on Advanced Trends in Radioelectronics, Telecommunications and Computer Engineering (TCSET). Lviv, 294–297. https://doi.org/10.1109/tcset64720.2024.10755561
9. Hvozdeva, I., Myrhorod, V., Budashko, V., Shevchenko, V. (2020). Problems of Improving the Diagnostic Systems of Marine Diesel Generator Sets. 2020 IEEE 15th International Conference on Advanced Trends in Radioelectronics, Telecommunications and Computer Engineering (TCSET). Slavske, 350–354. https://doi.org/10.1109/tcset49122.2020.235453
10. Budashko, V., Shevchenko, V. (2018). Synthesis of the Management Strategy of the Ship Power Plant for the Combined Propulsion Complex. 2018 IEEE 5th International Conference on Methods and Systems of Navigation and Motion Control (MSNMC). Kyiv, 106–109. https://doi.org/10.1109/msnmc.2018.8576266
11. Budashko, V., Hvozdeva, I., Onishchenko, O., Shevchenko, V., Kudelkin, R. (2020). Improvement of the operation for electromechanical system under non-permanent loading. 2020 IEEE 15th International Conference on Advanced Trends in Radioelectronics, Telecommunications and Computer Engineering (TCSET). Slavske, 35–39. https://doi.org/10.1109/tcset49122.2020.235588
12. Budashko, V. (2020). Thrusters Physical Model Formalization with regard to Situational and Identification Factors of Motion Modes. 2020 International Conference on Electrical, Communication, and Computer Engineering (ICECCE). Istanbul, 1–6. https://doi.org/10.1109/icecce49384.2020.9179301
13. Budashko, V., Obniavko, T., Onishchenko, O., Dovidenko, Y., Ungarov, D. (2020). Main Problems of Creating Energy-efficient Positioning Systems for Multipurpose Sea Vessels. 2020 IEEE 6th International

Conference on Methods and Systems of Navigation and Motion Control (MSNMC). Kyiv, 106–109. https://doi.org/10.1109/msnmc50359.2020.9255514

14. Budashko, V., Shevchenko, V. (2021). The synthesis of control system to synchronize ship generator assemblies. Eastern-European Journal of Enterprise Technologies, 1 (2 (109)), 45–63. https://doi.org/10.15587/1729-4061.2021.225517
15. Budashko, V., Shevchenko, V. (2021). Solving a task of coordinated control over a ship automated electric power system under a changing load. Eastern-European Journal of Enterprise Technologies, 2 (2 (110)), 54–70. https://doi.org/10.15587/1729-4061.2021.229033
16. Budashko, V. Diagnosis of the Technical Condition of High-Tech Complexes by Probabilistic Methods [Text] / V. Budashko, I. Hvozdeva, V. Shevchenko, V. Myrhorod, A. Sandler, O. Glazeva // 2022 IEEE 16th International Conference on Advanced Trends in Radioelectronics, Telecommunications and Computer Engineering (TCSET), Slavske, 22-26 Feb. 2022, Ukraine: IEEE TCSET 2022. – P. 7-14. Doi: https://doi.org/10.1109/TCSET49122.2020.235588
17. Budashko, V., Sandler, A., Shevchenko, V. (2022). Optimization of the control system for an electric power system operating on a constant-power hyperbole. Eastern-European Journal of Enterprise Technologies, 1 (8 (115)), 6–17. https://doi.org/10.15587/1729-4061.2022.252172
18. Budashko, V., Sandler, A., Shevchenko, V. (2022). Diagnosis of the Technical Condition of High-tech Complexes by Probabilistic Methods. TransNav, the International Journal on Marine Navigation and Safety of Sea Transportation, 16 (1), 105–111. https://doi.org/10.12716/1001.16.01.11
19. Sir Elkhatem, A., Naci Engin, S. (2022). Robust LQR and LQR-PI control strategies based on adaptive weighting matrix selection for a UAV position and attitude tracking control. Alexandria Engineering Journal, 61 (8), 6275–6292. https://doi.org/10.1016/j.aej.2021.11.057
20. Furmanik, M., Konvičný, D., Rafajdus, P. (2023). Low-Speed Sensorless Control for Six-Phase PMSM Based on Magnetic Anisotropy. Transportation Research Procedia, 74, 892–899. https://doi.org/10.1016/j.trpro.2023.11.222
21. Budashko, V., Sandler, A., Khniunin, S., Bogach, V. (2024). Design of the predictive management and control system for combined propulsion complex. Eastern-European Journal of Enterprise Technologies, 5 (2 (131)), 90–102. https://doi.org/10.15587/1729-4061.2024.313627
22. van Goor, P., Hamel, T., Mahony, R. (2023). Constructive Equivariant Observer Design for Inertial Navigation. IFAC-PapersOnLine, 56 (2), 2494–2499. https://doi.org/10.1016/j.ifacol.2023.10.1229
23. Hemalatha, N., Venkatesan, S., Kannan, R., Kannan, S., Bhuvanesh, A., Kamaraja, A. S. (2024). Sensorless speed and position control of permanent magnet BLDC motor using particle swarm optimization and ANFIS. Measurement: Sensors, 31, 100960. https://doi.org/10.1016/j.measen.2023.100960
24. Sagin, S. V., Semenov, O. V. (2016). Motor Oil Viscosity Stratification in Friction Units of Marine Diesel Motors. American Journal of Applied Sciences, 13 (2), 200–208. https://doi.org/10.3844/ajassp.2016.200.208
25. Lang, X., Mao, W. (2020). A semi-empirical model for ship speed loss prediction at head sea and its validation by full-scale measurements. Ocean Engineering, 209, 107494. https://doi.org/10.1016/j.oceaneng.2020.107494

26. Maidana, R. G., Kristensen, S. D., Utne, I. B., Sørensen, A. J. (2023). Risk-based path planning for preventing collisions and groundings of maritime autonomous surface ships. Ocean Engineering, 290, 116417. https://doi.org/10.1016/j.oceaneng.2023.116417
27. Myrhorod, V., Hvozdeva, I., Budashko, V. (2020). Multi-parameter Diagnostic Model of the Technical Conditions Changes of Ship Diesel Generator Sets. 2020 IEEE Problems of Automated Electrodrive. Theory and Practice (PAEP). Kremenchuk, 1–4. https://doi.org/10.1109/paep49887.2020.9240905
28. Sagin, S. V., Solodovnikov, V. G. (2017). Estimation of Operational Properties of Lubricant Coolant Liquids by Optical Methods. International Journal of Applied Engineering Research, 12 (19), 8380–8391.
29. Myrhorod, V., Gvozdeva, I., Budashko, V. (2022). Approximation - markov models of changes in the technical condition parameters of power and energy installations in long-term operation. Aerospace Technic and Technology, 4, 73–79. https://doi.org/10.32620/aktt.2022.4sup2.11
30. Nikolskyi, V., Budashko, V., Khniunin, S., Nikolskyi, M. (2018). Parametrization and identification of energy flows in the ship propulsion complex. 2018 14th International Conference on Advanced Trends in Radioelecrtronics, Telecommunications and Computer Engineering (TCSET). Slavske, 288–294. https://doi.org/10.1109/tcset.2018.8336205
31. Sandler, A., Budashko, V. (2022). Improving tools for diagnosing technical condition of ship electric power installations. Eastern-European Journal of Enterprise Technologies, 5 (5 (119)), 25–33. https://doi.org/10.15587/1729-4061.2022.266267
32. Budashko, V. V. (2021). Prospektive globale wissenschaftliche Trends: Modern technologies and concepts of researching for ship power plants of combined propulsion complexes. ScientificWorld-NetAkhatAV, 7 (7), 152. https://doi.org/10.30890/2709-2313.2021-07-07
33. Sandler, A., Budashko, V., Khniunin, S., Bogach, V. (2023). Improving the mathematical model of a fiber-optic inclinometer for vibration diagnostics of elements in the propulsion system with sliding bearings. Eastern-European Journal of Enterprise Technologies, 5 (5 (125)), 24–31. https://doi.org/10.15587/1729-4061.2023.289773
34. Boyko, A., Budashko, V., Yushkov, Y., Boyko, N. (2016). Synthesis and research of automatic balancing system of voltage converter fed induction motor currents. Eastern-European Journal of Enterprise Technologies, 1 (2 (79)), 22–34. https://doi.org/10.15587/1729-4061.2016.60544
35. Sáez, D., Cipriano, A. (1998). Fuzzy Linear Quadratic Regulator Applied to the Real Time Control of an Inverted Pendulum. IFAC Proceedings Volumes, 31 (4), 155–160. https://doi.org/10.1016/s1474-6670(17)42150-1
36. Budashko, V. (2015). Implementation approaches during simulation of energy processes for a dynamically positioned ship. Electrical Engineering & Electromechanics, 6, 14–19.
37. Budashko, V. V., Iushkov, E. A. (2015). Mathematic modeling of all-range controllers speed of thrusters for ship power plants in combined propulsion complexes. Electronic Modelin, 37 (2), 101–113. Available at: http://nbuv.gov.ua/UJRN/elmo_2015_37_2_10
38. Sagin, S. V., Kuropyatnyk, O. A., Zablotskyi, Yu. V. Gaichenia, O. V. (2022). Supplying of Marine Diesel Engine Ecological Parameters. Naše More, 69 (1), 53–61. https://doi.org/10.17818/nm/2022/1.7

39. Budashko, V. V. (2020). Ship's power plants of combined propulsion complexes: concepts, technologies, researching. Odesa: NU "OMA", 136.
40. Nikolskyi, V., Budashko, V., Khniunin, S., Nikolskyi, M. (2018). Development of a Computer System of Technical Condition for the Electric Podded Azimuth Thrusters. Information technologies and computer modelling. Ivano-Frankivsk, 157–160.